1 2 3	Grain size dependent magnetic discrimination of Iceland and south Greenland terrestrial sediments in the northern North Atlantic sediment record
4	
5	
6	Robert G. Hatfield ^{1†} , Joseph S. Stoner ¹ , Brendan T. Reilly ¹ , Frank J. Tepley III ¹ , Benjamin H. Wheeler ¹ , and
7	Bernard A. Housen ² .
8	
9	¹ College of Earth, Ocean, and Atmospheric Science, Oregon State University, Corvallis, Oregon, 97331,
10	USA.
11	
12	² Geology Department, Western Washington University, Bellingham, Washington, 98225, USA.
13	
14	
15	[†] Corresponding author. <u>rhatfield@ceoas.oregonstate.edu</u>
16	

Abstract

17

18

19

20

21

22

23

24

25

26

27

28

29

30

31

32

33

34

35

We use isothermal and temperature dependent in-field and magnetic remanence methods together with electron microscopy to characterize different sieved size fractions from terrestrial sediments collected in Iceland and southern Greenland. The magnetic fraction of Greenland silts (3-63 μm) and sands (>63 μm) is primarily composed of near-stoichiometric magnetite that may be oxidized in the finer clay (<3 µm) fractions. In contrast, all Icelandic fractions dominantly contain titanomagnetite of a range of compositions. Ferrimagnetic minerals preferentially reside in the silt-size fraction and exist as fine single-domain (SD) and pseudo-single-domain (PSD) size inclusions in Iceland samples, in contrast to coarser PSD and multi-domain (MD) discrete magnetites from southern Greenland. We demonstrate the potential of using magnetic properties of the silt fraction for source unmixing by creating known endmember mixtures and by using naturally mixed marine sediments from the Eirik Ridge south of Greenland. We develop a novel approach to ferrimagnetic source unmixing by using low temperature magnetic susceptibility curves that are sensitive to the different crystallinity and cation substitution characteristics of the different source regions. Covariation of these properties with hysteresis parameters suggests sediment source changes drive the magnetic mineral variations observed in Eirik Ridge sediments since the last glacial maximum. These observations assist the development of a routine method and interpretative framework to quantitatively determine provenance in a geologically realistic and meaningful way and assess how different processes combine to drive magnetic variation in the North Atlantic sediment record.

36

37

38

39

Keywords:

Source Unmixing, Environmental Magnetism, North Atlantic, Iceland, Greenland, Provenance.

1. Introduction

Marine sediments from the Northern North Atlantic (NNA) consistently provide high quality paleomagnetic and environmental magnetic records (Stoner et al., 1996; Channell and Lehman, 1997; Kissel et al., 1999; Watkins and Maher, 2003; Kissel, 2005; Hatfield et al., 2016). This quality is often attributed to an abundance of ferrimagnetic minerals that originate from mid ocean ridge volcanism and subglacial erosion of crystalline basement that surrounds the NNA (e.g. Watkins and Maher, 2003). These grains are efficiently transported from their source regions to the ocean in subglacial outwash or icebergs and are (re)distributed by down slope mass transport and by surface and deep-ocean currents (e.g. Robinson, 1986; Stoner et al., 1996; Kissel et al., 1999; Watkins and Maher, 2003; Kissel, 2005). Due to minimal magnetic mineral diagenesis (e.g. Robinson et al., 2000; Karamura et al., 2012), these minerals retain a primary signature reflecting their source (e.g. Watkins and Maher, 2003; Hatfield et al., 2013) and their transport/depositional history (e.g. Robinson, 1986; Stoner et al., 1996; Kissel et al., 1999; Kissel, 2005).

Downcore variations in bulk magnetic properties can be grouped into distinct spatial patterns across the NNA (e.g. Kissel, 2005). Peaks in magnetic susceptibility and coarsening of magnetic grain size are often interpreted as increased delivery of larger lithic grains from glacial marine processes, either IRD (i.e., Robinson, 1986) or overflows associated with down slope transport (i.e., Stoner et al., 1996), and/or as stronger bottom currents resulting in enhanced sediment transport (e.g. Kissel et al., 1999; Snowball and Moros, 2003). Correlation of bulk magnetic properties to independent datasets sensitive to transportation/depositional processes (e.g. Robinson 1986; Stoner et al., 1996; Channell et al., 2016) or to climatic variations observed in Greenland ice cores (that are generally thought to reflect Atlantic Meridional Overturning Circulation; e.g. Rasmussen et al., 1997; Kissel et al., 1999; Snowball and Moros, 2003), have reinforced transport driven explanations for magnetic mineral variations. In contrast, changes in source are often overlooked as fundamental drivers of downcore magnetic variability,

despite their role in controlling the abundance, mineralogy, and grain size of the magnetic materials available for transport. This has resulted from difficulties in the subtle discrimination of ferrimagnetic minerals using bulk environmental magnetic techniques (e.g. Thompson and Oldfield, 1986). In practice, unless non-ferrimagnetic contributions are routinely identified, sediment sources to NNA sediment records are frequently considered relatively uniform, despite being a convolution of source and transport processes. Accordingly, methods capable of robustly discriminating ferrimagnetic source variability from transport driven changes are required.

Magnetic properties of terrestrial and marine sediments from the NNA exhibit strong physical grain size dependence (Hatfield et al., 2013, 2016). For example, non-cohesive silts (10-63 μ m) from Greenland and Iceland, two large NNA terrestrial sediment sources, possess 2-5 times the mass-specific magnetic susceptibility (χ) values of fine silt/clay (<10 μ m) or sand (>63 μ m) fractions (Hatfield et al., 2013). While M_{rs}/M_s values (the ratio of saturation remanence [M_{rs}] to saturation magnetization [M_s] as a proxy for ferrimagnetic grain size) of Iceland clays (<3 μ m; M_{rs}/M_s range = 0.26-0.46), silts (3-63 μ m; 0.20-0.32), sands (>63 μ m; 0.19-0.31) and Greenland clays (0.10-0.33) are all similar, Greenland silts (0.03-0.15) and sands (0.02-0.14) are magnetically coarser and distinct from all Icelandic fractions (Hatfield et al., 2013). By restricting analysis to the silt-size fraction, Hatfield et al. (2013, 2016) demonstrated that the relative contribution of terrestrial sources could be determined and isolated relative to sediment transport/depositional processes that dictate sediment texture. However, while this methodology implied source variability may be an important driver of bulk NNA ferrimagnetic records (Hatfield et al., 2013, 2016), the origins of the observed variance in terrestrial samples (Hatfield et al., 2013) or marine sediments (Hatfield et al., 2016) are still unclear and have not sufficiently been explored.

To better understand the discrimination afforded between Iceland and Greenland terrestrial sources and the implications they have for driving bulk NNA variability, we build upon the research of

Hatfield et al. (2013) in four ways. First we expand the terrestrial χ and M_{rs}/M_s dataset through the measurement of 84 new sediment fractions from Iceland and Greenland. Second, using the same sediment samples as Hatfield et al. (2013) we make detailed temperature, frequency, and field dependent magnetic measurements and electron microscopy and energy dispersive spectroscopy (EDS) observations. This array of measurements allow an understanding of 1) why and how (sub)micron size ferrimagnetic grains exist in Icelandic silt and sand fractions, 2) what (if any) magnetic mineral variation exists between the distinct geological terranes, and 3) further the discrimination of the particle-size specific magnetic character of these sources. Next, we investigate unmixing of magnetic concentration, magnetic grain size, and magnetic mineralogy in the silt-size fraction through the measurement of known mixtures in order to investigate how these sources might behave in mixed sedimentary systems (e.g. marine sediment cores). Finally, we compare marine sediments to terrestrial end-members and mixtures and discuss implications for source-sink process interpretations in a geologically realistic and meaningful context.

2. Samples and Methods

2.1 Sample locations and sample preparation

The collection of Greenland and Iceland glacio-fluvial sediment samples is previously detailed in Hatfield et al. (2013); sampling locations and geological terrane boundaries are summarized in Fig. 1. Iceland and east-central Greenland are mainly composed of tholeiitic basalts, transitional alkali basalts, and alkali olivine basalts of Neogene and Paleogene age with regional variations encompassing ultramafic to rhyolitic compositions (e.g. Jakobsson, 1972; Pedersen et al., 1997). The Precambrian rocks of southern Greenland can be sub-divided into three geological terranes that extend roughly west-east and outcrop from under the ice sheet along the coastal margins (Fig. 1). The Ketilidian Mobile Belt (KMB)

is composed of juvenile Proterozoic crust consisting of voluminous granitic intrusions, while the Archean Block (AB) and Nagssugtoqidian Mobile Belt (NMB) are dominated by Archean age gneisses and granites that remained undeformed (AB) or were later metamorphosed during the Proterozoic (NMB) (Fig. 1; Korstgård et al., 1987; Escher and Pulvertaft, 1995). Although most sampling sites are located in the south and west of Greenland (Fig. 1) previous studies have shown it is reasonable to consider these as geological analogues for outcrops within the same terrane in east Greenland (Colville et al., 2011; Reyes et al., 2014; Hatfield et al., 2016). Hatfield et al. (2013) reported x data on five fine silt/clay and silt fractions and hysteresis data on clay, silt, and sand fractions from 67 locations in Greenland and 11 from Iceland. We augment this dataset with x measurements of clay, silt, and/or sand from 79 new and existing locations (61 in Greenland, 18 in Iceland) and hysteresis measurements from 41 new locations (28 in Greenland, 13 in Iceland). All samples were collected during the same field programs as those presented in Hatfield et al. (2013). The sand fraction was isolated by wet sieving at 63 µm and the clay (<3 µm) and silt (3-63 µm) fractions were separated according to Stokes law following Hatfield et al. (2013). To assess the linear additivity of magnetic properties, fifteen mixtures of Iceland and Greenland sediments were created by mixing an Iceland silt sample and a silt sample from each of the three terranes of southern Greenland in five weight proportions (90:10, 80:20 70:30, 50:50, and 30:70). All samples were weighed and either pressed in gelatin caps for Magnetic Property Measurement System (MPMS) and Vibrating Sample Magnetometer (VSM) measurements, placed in glass vials for temperature dependent magnetic susceptibility measurements, or immobilized in 8cc cubes for measurements of room temperature magnetic susceptibility.

131

132

133

134

111

112

113

114

115

116

117

118

119

120

121

122

123

124

125

126

127

128

129

130

2.2 Magnetic measurements

Room temperature magnetic susceptibility measurements were made at 470 Hz in a field of ~80 Am⁻¹ on a Bartington MS2B susceptometer (n=233) at the Paleo-and-Environmental Magnetism Laboratory at

Oregon State University. Temperature dependent remanence and frequency dependent susceptibility measurements were made using a Quantum Design MPMS. Changes to the low temperature induced saturation isothermal remanent magnetization (LTSIRM) during warming were recorded after cooling from room temperature using FC and ZFC protocols (e.g. Bilardello and Jackson, 2013). For the Zero-Field Cooled (ZFC) remanence measurements the sample was cooled in a zero field from 300-10 K, a LTSIRM was imparted (2.5 T at 10 K), and the remanence was measured at 5 K increments on warming from 10-300 K. For the field cooled (FC) protocol the sample was cooled to 10 K in the presence of a constant 2.5T field, after which the same response to warming was measured as in the ZFC protocol. Forty-three clay, silt, and sand samples were measured for ZFC, one silt sample from Iceland and each of the three terranes of southern Greenland were measured for FC remanence. Frequency dependent susceptibilities (χ_{fd}) for one Iceland clay, silt, and sand sample and one Greenland AB clay and silt sample were measured during warming from 10-300 K at five frequencies (1, 5.6, 32, 177, 997 Hz) in a field of 240 Am⁻¹. M_s, M_{rs}, and coercivity (H_c) data of 97 terrestrial sediment fractions and 15 silt mixtures were derived from major hysteresis loops measured to a saturating field of 1000 mT and corrected for paramagnetic contributions using the high field slope above 800 mT. The coercivity of remanence (H_{cr}) was determined by direct current demagnetization of a 1000 mT IRM in 2.5 mT steps. First order reversal curves (FORCs) are composed of 104 individual FORC measurements taken with an averaging time of 0.5 seconds and a peak field of 200 mT (n = 9) and were processed using smoothing factors of 2-3 using the FORCinel software of Harrison and Feinberg (2008). Hysteresis loops, Hcr, and FORCs were measured on a Princeton Measurements Corporation VSM. High temperature χ of Iceland and Greenland silt and sand fractions (n = 29) were measured on a Kappabridge KLY-2 at a frequency of 920 Hz in a 300 Am⁻¹ field. Samples were measured in air every 3-4°C during heating from room temperature to 650°C and during cooling from 650°C to 50°C. χ values recorded during heating and cooling were smoothed using a 5-point running average and were divided by values of χ at 50°C to produce

135

136

137

138

139

140

141

142

143

144

145

146

147

148

149

150

151

152

153

154

155

156

157

normalized high-temperature χ values. All FORC, χ_{fd} , and high-temperature χ measurements were made at the Institute for Rock Magnetism at the University of Minnesota in Minneapolis. Low-temperature χ measurements (n = 25) were acquired by cooling the sample in liquid nitrogen to ~80 K and measuring χ every 1-2 K during warming to ~273 K on a Kappabridge KLY-2 at a frequency of 920 Hz in a 300 Am⁻¹ field. M_s , M_{rs} , H_c , and low-temperature χ properties of the terrestrial samples and mixtures were measured at the Pacific Northwest Paleomagnetic Laboratory at Western Washington University.

2.3 Electron microprobe analysis

One silt and one sand sample from Greenland and Iceland were prepared for electron microprobe analysis (EMP) at the Electron Microprobe Laboratory at Oregon State University. Samples were mounted in epoxy resin and polished using a 1- μ m diamond cloth before being loaded into the Cameca SX-100 Electron Microprobe. Samples were analyzed using 15 keV accelerating voltage, 30 nA sample current, and 1 μ m beam diameter. Back-scattered electron (BSE) images were obtained using the same instrument using the CAMECA Peak Site software.

3. Results

3.1 Room temperature magnetic susceptibility

For each Greenlandic terrane the silt fraction has higher median χ values than either the clay or the sand fraction indicating that the silt fraction is enriched in magnetic minerals (Fig. 2a). For the Iceland samples, the median χ of the clay fraction is ~5 times lower than both the median silt and sand fractions suggesting that magnetic mineral concentrations in Icelandic silts and sands are not as sensitive to clastic size variations as those from Greenland (Fig. 2a). These findings are consistent with

previous data that show homogeneity in χ across six different Icelandic silt and sand size fractions and lower Greenland and Iceland clay χ values relative to their coarser fractions (Hatfield et al., 2013).

3.2 Hysteresis and coercivity of remanence measurements

Iceland and Greenland median M_{rs} values (Fig. 2b) are higher in the silt fraction than in the clay fraction implying greater enrichment of ferrimagnetic remanence carrying minerals (e.g (titano)magnetite, maghemite) in the silt fraction. H_c (Fig. 2c) and H_{cr} (Fig. 2d) are sensitive to magnetic grain size and magnetic mineralogy and are consistently higher in the clay fraction than in the silt or sand fractions across all four terranes. While clay H_c and H_{cr} values are similar regardless of source, silt and sand, H_c and H_{cr} values are lower for the Greenlandic samples than the Icelandic samples and become progressively lower from KMB through AB to NMB (Fig. 2c, 2d). When silt hysteresis loops from each terrane are normalized and averaged, Iceland samples possess the widest loops, lowest H_{cr}/H_c ratios, and highest values of M_{rs}/M_s, H_c, and H_{cr} (Fig 2e). On the other hand, Greenland loops are narrower (Fig. 2f-h), and narrow from the KMB, through the AB, with the NMB possessing the narrowest loops, highest H_{cr}/H_c ratios, and lowest values of M_{rs}/M_s, H_c, and H_{cr}.

Icelandic clays have slightly higher M_{rs}/M_s values (M_{rs}/M_s clay range 0.24-0.49) than their corresponding silt (0.16-0.35) or sand (0.16-0.40) fractions indicating a finer magnetic grain size assemblage. However, when combined in Day Plot space (Day et al., 1977) all fractions show considerable overlap in a region characteristic of relatively fine Pseudo-Single Domain (PSD) ferrimagnetic grain sizes (Fig. 2i) suggesting that variation between samples is greater than variation between fractions. While Greenland clays have M_{rs}/M_s values (0.07-0.28) similar to Iceland fractions, the lower H_{cr}/H_c ratios of Iceland clays mean they plot to the right of Greenland clays in Day plot space (Fig. 2i, 2j). Higher H_{cr}/H_c values in Iceland fractions could be indicative of higher superparamagnetic (SP) concentrations and/or a greater proportion of titanomagnetite relative to magnetite (Dunlop, 2002).

Greenland silts and sands have lower M_{rs}/M_s and higher H_{cr}/H_c ratios compared to Iceland fractions and Greenland clays, and occupy coarse PSD and Multi-Domain (MD) regions on a Day Plot (Fig. 2i). Within Greenland, KMB silts and sands have higher M_{rs}/M_s values than those from NMB suggesting a finer average magnetic grain size population in this southernmost terrane (Fig. 2i). The new combined dataset (Fig. 2j) reinforces and extends the source discrimination inferred by Hatfield et al. (2013) with M_{rs}/M_s values of Iceland silts being magnetically finer (M_{rs}/M_s median = 0.26; range = 0.16-0.36) and distinct from the coarser silts (M_{rs}/M_s median = 0.06; range = 0.02-0.15) of south Greenland (Fig. 2j).

3.3 High temperature magnetic susceptibility

 χ values of Greenland silts and sands are generally stable during heating from 20 to 540°C; above ~540°C χ values decline sharply associated with the Curie temperature (T_c) (Fig. 3b-d, 3g, 3h). Using the differential method to estimate T_c (Tauxe, 1998), average peak d^2M/dT^2 values of the Greenland silts and sands are 570 °C (\pm 20 and 24 °C as 2 std. deviations (2σ) respectively; Fig. 3i-j). This is consistent with magnetite being the dominant magnetic mineral (Thompson and Oldfield, 1986; Moskowitz, 1993). Variability in χ below T_c during heating is greater in the Greenland silt fraction than in the sand fraction (Fig. 3g-h). While the heating curves of the sand fraction are largely retraceable during cooling, the cooling curves of the silt fraction are significantly lower (Fig. 3b-d). Greater χ variability in the silt fraction suggests greater alteration with temperature that can possibly result from SP unblocking and/or from greater thermal conversion of minor magnetic phases such as maghemite (e.g. Oches and Banerjee, 1996) or hematite (e.g. Stacey and Banarjee, 1974). Alternatively, the two fractions could have similar compositions with greater alteration resulting from higher reactive surface-volume ratios in the silt fraction and/or additional protection from oxidation/alteration by inclusion of the ferrimagnetic assemblage in silicate sands (e.g. Chang et al., 2016).

Iceland silts and sands show more complex decreases in χ during heating (Fig. 3a, 3e, 3f) with T_c covering wider temperature ranges between 100-200 °C and 425-600 °C (see insets in Fig. 3i-j). Lower T_c is consistent with titantomagnetite (Fe_{3-x} Ti_xO₄, $0 \le x \le 0.6$, TM0-TM60) while multiple peaks in d^2M/dT^2 values suggest variable cation substitution (Moskowitz, 1993; Lattard et al., 2006) of the Iceland samples. Iceland silt and sand χ cooling curves are frequently higher than the heating curves (Fig. 3a). This signature can result from exsolution of titanomagnetite during heating and/or thermal alteration of iron bearing silicates to form new ferrimagnetic minerals.

3.4 Low temperature and frequency dependence of magnetic susceptibility

For temperatures between 80 and 273 K clay χ values (Fig. 4a-b) are lower than silt χ values (Fig. 4c-d) across all four terranes. The low-temperature Greenland silt χ profiles are dominated by a rapid increase in χ between 100-130 K (Fig. 4d), consistent with the Verwey transition (T_v) and isotropic point (e.g. Muxworthy and McClelland, 2000; Carter-Stiglitz et al., 2006) of stoichiometric magnetite (e.g. Özdemir et al., 1993, 2002; Moskowitz et al., 1998). This signature is somewhat echoed in the Greenland clays, though the relative magnitude of the 100-130 K increase in χ is either suppressed or absent, resulting in flatter χ profiles between 80-273 K (Fig 4b). When χ values are normalized to their 273 K χ values (χ/χ_{273K}) and compared to similar profiles of known compositions (Moskowitz et al., 1998), Greenland silt χ/χ_{273K} profiles closely follow the TM0 curve (Fig. 4e), consistent with a magnetite dominated interpretation. Peak χ/χ_{273K} values occur between 125-130 K and on average are 1.13 (± 0.03 as 2 σ ; Fig. 4e) with the subsequent decreases in χ/χ_{273K} between the T_v and 273 K a characteristic signature of MD sized magnetite (Thompson and Oldfield, 1986). Suppression or absence of a T_v in Greenland clay may result from a combination of finer grained magnetite and/or oxidation of that population in the clay fraction (e.g. Özdemir et al., 1993).

Iceland clay and silt fractions lack a T_v and peak χ values are only attained at 273 K resulting in a range of flat, steadily increasing, or concave up profile shapes that steepen at higher temperatures (Figs. 4a, 4c). Steady increases in χ with increasing temperature is a common feature of Ti-poor titanomagnetite and oxidized magnetite (Özdemir et al., 1993; Moskowitz et al., 1998), while steep concave up profiles above ~175 K are typical of Ti-rich (TM40-TM60) titanomagnetite (Moskowitz et al., 1998; Fig. 4f). χ/χ_{273K} profiles of Iceland silts generally fall between the TM19-TM60 curves of Moskowitz et al. (1998; Fig. 4f). Individual profiles do not follow any single TM-curve, but instead have characteristics of multiple curves (Fig. 4f) suggesting a range of mineralogical compositions and greater mineralogical complexity in these glacio-fluvial samples than the magnetite dominated Greenlandic silts.

 χ_{fd} [χ_{fd} = ($\chi_{(1Hz)} - \chi_{(32Hz)}$)/ $\chi_{(1Hz)}$ x 100] is relatively high across all Iceland fractions peaking at ~5 % for the clay fraction and ~8 % for the silt and sand fractions between ~60-70 K (Fig. 5). Peaks in χ_{fd} between ~60-70 K can be attributed to thermally activated electron hopping that occurs in titanomagnetite (Walz et al., 1997; Carter-Stigliz et al., 2006) while relatively high χ_{fd} values of ~3-5 % that increase with increasing temperature above 100 K indicate the presence of both SP and SD grains (e.g. Worm, 1998; Worm and Jackson, 1999). Above the T_V Greenland clay and silt χ_{fd} values are relatively low and stable and average 1.2 % and 0.5 %, respectively, indicating little to no significant SP populations in the Greenland clay and silt sample.

3.5 Zero field cooled and field cooled remanence

Greenland fractions show the greatest loss of IRM (Fig. 6d-f), and highest peaks in IRM' (Fig. 6g-i) between 100-120 K associated with the T_v in magnetite. Loss of remanence across the T_v ($\delta T_v = [M^{80K} - M^{150K}]/M^{80K}$; Moskowitz et al., 1993) is lower in Greenland clay ($\delta T_v = 0.2$) than in Greenland silt ($\delta T_v = 0.69$) or sand ($\delta T_v = 0.65$), likely resulting from non-stoichiometry due to oxidation and/or populations of fine SD size magnetic grains (Özdemir et al., 1993; Moskowitz et al., 1993). Greenland silt and sand fall in

the δT_v range observed for SD-PSD-MD size stoichiometric magnetite (0.64-0.86; Özdemir et al., 1993) while clay δT_v values are more consistent with those observed for surface oxidized magnetite (0.11-0.35; Özdemir et al., 1993). Increasing oxidation, estimated by z (where z is the fraction of initial Fe^{2+} oxidized to Fe^{3+}), acts to smear out low temperature remanence transitions and is almost absent for z > 0.3(Özdemir et al., 1993, 2002). A suppressed, but identifiable clay T_v allows us to suggest a potential upper limit (z < 0.3) of surface maghemitization of magnetite in the Greenland clay fraction. If we assume the Greenland silts and sands are dominated by (near-)stoichiometric magnetite (Figs. 3, 4, 5, 6) then retention of the 10 K imparted LTSIRM after warming to 300 K (LTSIRM_{300K/10K} = LTSIRM_{300K}/LTSIRM_{10K}) can be related to magnetic grain size variations (Özdemir et al., 1993, 2002). Greenland sand LTSIRM_{300K/10K} values (0.17 \pm 0.05 as 1 σ) are slightly lower than Greenland silt values (0.19 \pm 0.04) indicating a slightly coarser average magnetic grain size assemblage in the sand fraction (Fig. 6h-i), consistent with the Day Plot data (Fig 2i). KMB silts have higher LTSIRM_{300K/10K} values (0.32 \pm 0.05) than the AB (0.20 ± 0.02) or NMB (0.15 ± 0.06) samples suggesting a finer average magnetic grain size assemblage is associated with the KMB. ZFC remanence is higher than FC remanence in the AB and NMB silt, while ZFC and FC values for the KMB silt sample are relatively similar (Fig. 6k-m) resulting in RLT values (where R_{LT} = FC SIRM_{20K}/ZFC SIRM_{20K}; Smirnov, 2009) of 0.78 (NMB), 0.83 (AB), and 1.01 (KMB) respectively. Comparison of these R_{LT} values to those of synthetic magnetite (Smirnov, 2009) suggest the KMB sample contains fine PSD-size magnetite around 1 µm, while lower values of the AB and NMB silt suggest coarser PSD and MD grains in the tens of microns range (Smirnov, 2009).

275

276

277

278

279

280

281

282

283

284

285

286

287

288

289

290

291

292

293

294

295

296

297

298

ZFC profiles of all Iceland fractions are characterized by steep initial loss of remanence between \sim 10-30 K (Fig. 6a-c) followed by relatively linear demagnetization profiles above \sim 50 K. None of the Icelandic fractions display an abrupt loss of remanence associated with stoichiometric magnetite or Tipoor titanomagnetite (e.g. Moskowitz et al., 1998) (Fig. 6a-c). Accordingly δT_{ν} values of Iceland fractions are 3-6 times lower than Greenland silt and sand fractions. Continued loss of remanence above 150 K

yields relatively high values of δM ($\delta M = [M^{150K} - M^{300K}]/M^{150K}$; Moskowitz, 1993) which can be characteristic of both Ti-rich (TM>40) titanomagnetite and SP grains that continue to unblock with increasing temperature (Moskowitz, 1993). LTSIRM_{300K}/LTSIRM_{10K} values are relatively high in Iceland fractions, and are higher in the clay fraction (0.47 ± 0.09) than the silt (0.35 ± 0.02), and sand (0.39 ± 0.07) fractions, likely reflecting a combination of greater cation-substitution (e.g. Moskowitz et al., 1998) and finer magnetic grain sizes compared to Greenland. Mineralogical differences between the Greenland and Iceland fractions prevent direct comparison of their R_{LT} values, but elevated FC over ZFC remanence in the Iceland silt ($R_{LT} = 1.2$) is consistent with an assemblage dominated by fine PSD and SD grains (Carter Stiglitz et al., 2006). Continued offsets in the Iceland ZFC and FC remanence datasets with warming to room temperature suggest that both Ti-rich mineralogies and SP grain populations contribute to the relatively high values of δM because if SP grains were absent then FC and ZFC remanence would be identical above the T_v (e.g. Özdemir et al., 1993; Moskowitz et al., 1998; Jackson et al., 2011). All magnetic and ratio data presented thus far are summarized in supplementary tables 1 and 2.

3.6 First order reversal curves (FORCs)

FORC diagrams are sensitive to variations in coercivity and most frequently are interpreted in terms of ferrimagnetic grain size (e.g. Roberts et al., 2000; Egli et al., 2010). Iceland and Greenland clay samples are characterized by a tightly defined intensity structure with nearly oval contours that spreads laterally along the central Hc axis; the Iceland and KMB clay also have a distinct negative region in the lower left of the FORC diagram (Fig. 7a, 7d). These signatures are characteristic of non-interacting SD grains (e.g. Egli et al., 2010) and initially appear similar to those frequently interpreted as bacterial magnetosomes in marine sediments (e.g. Roberts et al., 2000; Ludwig et al., 2013). However, peak coercivity of these terrestrial clay fractions is up to 20mT lower and the coercivity distribution is wider

than those expected for magnetosomes (Fig.7; e.g. Ludwig et al., 2013; Channell et al., 2016). These clay fractions are instead more consistent with abiotic detrital SD grains that have been found to exist as inclusions within larger host grains (e.g. Ludwig et al., 2013). Recognition of this terrestrially sourced central-ridge type SD signature is important as it can potentially contribute to SD end-member signatures in NNA marine sediment records that are frequently interpreted to infer populations of bacterial magnetosomes (e.g. Ludwig et al., 2013; Channell et al., 2016).

Iceland silt and sand samples possess a more rounded, sometimes truncated, closed contour structure. In addition, they have lower peak coercivity than clay fractions and possess triangular contour lines that intersect the vertical axis and are indented on the lower branch (Fig. 7e-f). These FORC characteristics are consistent with PSD-size grains (e.g. Roberts et al., 2000). The KMB silt and sand sample have similar peak coercivity and indented lower contour branches, but also possess a broader intensity distribution that extends higher up the vertical axis suggesting the presence of coarser PSD grains (Fig. 7e-f) than in the Iceland samples or KMB clay fraction. Lower peak coercivity in the NMB silts and sands and greater spread along the Hu axis is indicative of coarser PSD and MD size grains (e.g. Roberts et al., 2000). These FORC interpretations are consistent with those derived from the hysteresis data and low temperature remanence data, suggesting that clays contain the finest magnetic grain sizes, that magnetic grain size scales to a greater extent with physical grain size across southern Greenland, and that silts and sands from Iceland are magnetically finer than those from the KMB which are finer than those from the NMB. However, FORCs also highlight subtle magnetic grain size variation across Iceland fractions with greater SD populations in the clay size fraction relative to silt and sand.

3.7 Electron microscopy and electron dispersive spectroscopy

Electron backscatter images are sensitive to atomic mass with bright (dark) grayscale regions possessing relatively high (low) atomic numbers (Fig. 8a, 8c). Energy dispersive spectrometry (EDS)

spectra of the brightest Greenland silt grains returns two energy peaks related to Fek α and Fek β (Fig. 8b). This suggests that iron is the single dominant element and, because each silt grain shows relatively little gray scale variation (Fig. 8a), that these iron-rich minerals (magnetite) exist as discrete grains. In contrast the Iceland silts contain a wider range of brightness values within individual grains, indicating greater elemental and mineralogical heterogeneity (Fig. 8c). The brightest regions within these sand grains are also dominated by iron, but are accompanied by similar size peak counts of titanium (Fig. 8b) supporting the magnetic data that suggest titanomagnetite is an important remanence carrying mineral in Icelandic samples. Instead of occupying whole grains these Fe-Ti rich regions exist as smaller inclusions within larger, non-ferrimagnetic, polycrystalline host grains (Fig. 8c).

4. Discussion

4.1 Discrimination of NNA sources.

This detailed rock magnetic and electron microscopic dataset highlights a range of magnetic behaviors that associate with different sediment size fractions from Iceland and three terranes of southern Greenland. Icelandic clay, silt, and sand fractions are dominated by experimental behavior consistent with relatively fine grained (SP-SD-PSD) Ti-rich and Ti-poor titanomagnetite that are frequently reported as the major magnetic mineralogical constituent of mid-ocean ridge and Icelandic basalt (Gee and Kent, 1999; Muxworthy et al., 2011). Variation in titanomagnetite composition within and between samples (Fig. 4f) likely reflects variability in regional geology and integration of this variability within these glacio-fluvial samples. Basalt cools relatively quickly restricting crystal size and resulting in a relatively fine-grained magnetic grain size assemblage within Icelandic bedrock samples (e.g. Radhakrishnamurty, 1990; Muxworthy et al., 2011). Sub-micron and few micron size SD and PSD grains appear to survive mechanical weathering processes (e.g. glacial crushing, grinding etc) as

inclusions within larger polycrystalline clasts (Fig. 8c) during generation of silt and sand size fractions.

Polycrystalline compositions effectively explain why magnetic grain size appears independent of physical grain size across five different silt-size fractions (Hatfield et al., 2013) with SD and fine PSD size magnetic grains are present in Iceland silts and sands.

Greenlandic silts and sands contain near-stoichiometric discrete magnetite grains that span a coarser PSD-MD magnetic grain size range. Similar to Iceland, the clay fractions have lower ferrimagnetic content and finer magnetic grain sizes than the silt and sand size fractions (Figs. 2, 7), while the finest SD and fine PSD size magnetite grains may be partially oxidized to maghemite (Fig. 6). The greater range of magnetic grain sizes in Greenlandic silt and samples likely results from the granitic igneous intrusions (KMB) and granites and gneisses (AB and NMB) that cooled at slower rates and over longer time periods (e.g., 1–7°C Ma⁻¹ for the NMB; Willigers et al., 2002) than the rapidly cooled basalts in Iceland. This results a greater range of PSD size (0.07-20 μm) and MD size (>20 μm) grains in the primary bedrock (e.g. Miki et al., 2009). Mechanical weathering efficiently liberates these ferrimagnetic grains leaving them as discrete entities in the silt-size fraction. The finest magnetic grains exist in the clay-size fraction of all terranes (Figs. 2, 7), potentially resulting from the natural exclusion of coarser PSD and MD size grains and/or the opposing surface-charge attraction of ultra-fine iron oxides to clay minerals (e.g. Galindo-Gonzalez et al., 2009). Particle size dependence of magnetic grain size is therefore a fundamental characteristic of south Greenland. The KMB terrane contains an additional magnetically fine-grain size population that is absent in the AB and NMB, providing a subtle difference to magnetically discriminate terranes within southern Greenland.

4.2 Endmember unmixing

370

371

372

373

374

375

376

377

378

379

380

381

382

383

384

385

386

387

388

389

390

391

392

393

Our new data demonstrate that ferrimagnetic grains are enriched in the silt-size fraction, that magnetic grain size strongly scales with physical grain size in Greenland, and that magnetic mineralogy

and magnetic grain size of the silt-size fraction can discriminate these two sources. While clay also exhibits differences between source regions, their properties frequently overlap in endmember (EM) space, and differences are too subtle for unambiguous source discrimination (e.g. Figs. 2, 6, 7). Clay and silt often dominate the bulk sediment texture in NNA marine sediment cores, therefore magnetic homogeneity of the clay-size fractions could dilute any source discrimination afforded by the silt-size fraction in the bulk sediment. Lower concentration of ferrimagnetic grains in the clay-size fraction means this effect is dampened in the bulk sediment, however, unless armed with detailed particle-size distribution data, it can be difficult to estimate the relative effects of changing sediment texture (often driven by transport) from changes in sediment source(s) in bulk records. Restricting analysis to the silt-size fraction negates many of these issues. Therefore, to evaluate magnetic properties for source unmixing we now focus exclusively on the silt-size fraction.

Source unmixing relies on endmembers that behave linearly, or at least in a predictable way, when mixed (Dunlop, 2002; Heslop 2015). Although χ and hysteresis loops are largely assumed to be linearly additive in many different environments, this assumption is rarely explicitly tested. Here we compare the magnetic properties of mixtures comprised of known proportions of Icelandic and Greenlandic silt to the theoretical magnetic properties of these mixtures based on their EMs (Fig. 9a) assuming that magnetic susceptibility is linearly additive:

$$\chi_{\text{mix}} = f_{\text{grn}}(\chi)_{\text{grn}} + f_{\text{ice}}(\chi)_{\text{ice}}$$
 (eq. 1)

412 Where:

 $\chi_{mix} = \chi$ of the theoretical mixture

f = the fractional abundance of the Greenlandic (f_{grn}) and Icelandic (f_{ice}) endmember

 $(\chi) = \chi$ of the Greenlandic $[(\chi)_{grn}]$ and Icelandic $[(\chi)_{ice}]$ endmember

Each sample mixture plots on top of its equivalent χ_{mix} curve, demonstrating the linear additivity of χ over the full 80-273 K temperature range (Fig. 9a). While χ and the concentration dependent hysteresis parameters M_{rs} and M_s are linearly additive, ratios derived from them (e.g. χ/χ_{273K} or M_{rs}/M_s) follow a non-linear function if the two end-members have different intensities (e.g. Dunlop, 2002). Using the same EMs in Fig. 9a we adopt equation 14 in Dunlop (2002) to estimate χ/χ_{273K} (or M_{rs}/M_s) using:

 $\chi/\chi_{273K} = [f_{grn}(\chi)_{grn} + f_{ice}(\chi)_{ice}] / [f_{grn}(\chi_{273K})_{grn} + f_{ice}(\chi_{273K})_{ice}]$ (eq. 2)

Where:

 $\chi = \chi$ of the Greenlandic ($(\chi)_{grn}$) and Icelandic ($(\chi)_{ice}$) endmember at a given temperature $\chi_{273K} = \chi$ at 273 K for the Greenlandic ($(\chi_{273K})_{grn}$) and Icelandic ($(\chi_{273K})_{ice}$) endmember

Using this function our known mixtures reproduce the theoretical values within $\sim 5\%$ for both χ/χ_{273K} (Fig. 9b) and M_{rs}/M_s values (Fig. 9c), suggesting that proxies for magnetic concentration (Fig. 9a), magnetic mineralogy (Fig. 9b), and magnetic grain size (Fig. 9c) all appear appropriate to unmix NNA source contributions within a mixed sediment source system.

Variation in the magnetic grain size of the silt-size fraction has been used to determine sediment source changes to marine sediment core MD99-2227 from the Eirik Ridge south of Greenland (Fig. 1; Hatfield et al., 2016). This interpretation assumed that variations in M_{rs}/M_s of the silt-size fraction were dominantly driven by sediment source changes and that other potential influences (e.g. sediment diagenesis/authigenesis) were relatively unimportant (Hatfield et al., 2016). Our new data suggest that magnetic mineralogy, determined through χ/χ_{273K} , can also effectively discriminate source, providing an opportunity to independently check the provenance driven M_{rs}/M_s interpretation in MD99-2227. If source changes do dictate silt M_{rs}/M_s values, then silt χ/χ_{273K} profiles should track these contributions

accordingly. In contrast, variations in sediment sorting or contributions from additional geological, authigenic, or diagenetic sources would likely complicate this relationship.

To test this hypothesis we measured χ/χ_{273K} profiles and M_{rs}/M_s ratios of eight silts from MD99-2227 sampled between 23-6 ka during which the contribution of Greenland and Iceland sources varied significantly (Reyes et al., 2014; Hatfield et al., 2016). While Iceland EMs have larger variability than Greenland EMs, MD99-2227 χ/χ_{273K} and M_{rs}/M_s values plot between the two end-members (Fig. 10a, 10b). As we are interested in determining the Greenlandic contribution (f_{grn}) to each sample, we rewrite equation 2 such that:

$$f_{grn} = (C \times [(R_{sample} - R_{grn}) / (R_{ice} - R_{sample})] + 1)^{-1}$$
 (eq. 3)

449 Where:

C = Greenland EM concentration / Iceland EM concentration (χ_{273K} for χ/χ_{273K} , M_s for M_{rs}/M_s)

 $R = \chi/\chi_{273K}$ or M_{rs}/M_s of MD99-2227 sample (R_{sample}), Iceland EM (R_{ice}), and Greenland EM (R_{grn})

To quantify our uncertainty, we solve for $f_{\rm grn}$ 10,000 times, varying our choice of C, $R_{\rm grn}$, and $R_{\rm ice}$. In each iteration, $M_{\rm rs}/M_{\rm s}$ EMs were randomly sampled from a log-normal distribution fit to the terrestrial observations and $\chi/\chi_{\rm 273K}$ EMs were generated by randomly varying contributions of the measured $\chi/\chi_{\rm 273K}$ profiles from each source region. The Greenland to Iceland concentration ratio (C) was determined by averaging 1,000 $M_{\rm s}$ and χ values sampled from a log-normal distribution fit to the terrestrial dataset. For each $\chi/\chi_{\rm 273K}$ iteration the $f_{\rm grn}$ estimate is an average of 126 equally spaced $f_{\rm grn}$ estimates over the 125K-250 K temperature range.

Mean f_{grn} estimates derived from M_{rs}/M_s and χ/χ_{273K} are compared in Fig. 10c with bars denoting one standard deviation. Strong correlation between the two estimates (r = 0.94; Fig. 10c) indicates that magnetic mineralogy shifts accompany magnetic grain size changes in MD99-2227 silt, supporting the predominantly sediment source driven interpretation. However, in absolute terms $f_{grn} \chi/\chi_{273K}$ estimates

are higher than the f_{grn} M_{rs}/M_s estimates (Fig. 10c). Greater similarity between f_{grn} M_{rs}/M_s and independent isotope based estimates of source interpolated from the dataset of Reyes et al. (2014) (Fig. 10d) suggests χ/χ_{273K} over predicts Greenlandic contributions. f_{grn} M_{rs}/M_s and f_{grn} χ/χ_{273K} values can be reconciled by either changing the f_{grn} χ/χ_{273K} C term to a value of 3 (Fig. 10e) or by excluding the two Tirich χ/χ_{273K} profiles (Fig. 4) from the EM determination (Fig. 10f).

464

465

466

467

468

469

470

471

472

473

474

475

476

477

478

479

480

481

482

483

484

485

486

487

In our initial runs, the median C terms use χ and M_s values sampled from the terrestrial silt dataset (Fig. 2) and are 1.09 and 1.29, respectively. Comparison of the χ and M_s measurements do not show any systematic offset between the two concentration dependent datasets making it difficult to justify increasing the $f_{grn} \chi/\chi_{273K} C$ term by a factor of ~3 relative to that used in the $f_{grn} M_{rs}/M_s$ calculation. Excluding the two Ti-rich Iceland samples changes the χ/χ_{273K} profile shape and increases the average χ/χ_{273K} value of the Iceland EM, decreasing χ/χ_{273K} derived f_{grn} estimates as a result (Fig. 10f). While it is possible that our five χ/χ_{273K} curves under-sample the Iceland variability, Iceland and midocean ridge basalt are frequently enriched in Ti-rich mineralogies (e.g. Gee and Kent, 1999; Muxworthy et al., 2011) making this solution unlikely. An alternative explanation for this discrepancy is a third source of fine-grained Ti-poor or stoichiometric magnetite that is not captured by our terrestrial EMs but covaries with contributions of Icelandic material to maintain the strong relationship in Fig. 10c. Bacterial magnetosomes fulfill the magnetic description, but they likely reside in the clay-size fraction after separation (Hatfield, 2014) and it is difficult to explain why they would covary with Icelandic material. Instead, a third source of fine-grained magnetite from the Nordic seas or east Greenland shelf, as two large uncharacterized submarine sediment source regions, may integrate with Icelandic sourced material during transport along the path of the Deep Western Boundary Current (DWBC; Fig. 1). Due to its proximity to the NMB, the east Greenland shelf (Fig. 1) is likely dominated by a relatively coarse ferrimagnetic assemblage. In contrast, potential terrestrial sediment sources to the Nordic seas include Iceland, Jan Mayen, and the coastlines of northeastern Greenland and western Norway. If these sources

are dominated by relatively fine-grained magnetite then their transport through the Denmark Strait alongside Icelandic sourced material (Fig. 1) may help reconcile the $f_{\rm grn}$ estimates of the two endmembers. However, further work is required to better characterize the silt-size magnetic fingerprint of Nordic seas sediments before this can be concluded.

5. Conclusions

Detailed rock magnetic characterization of terrestrial sediments from Iceland and southern Greenland has guided a growing understanding of how to discriminate ferrimagnetic sources to the NNA. Measurement of specific size fractions permits isolation of certain properties and targeting of desirable characteristics for sediment provenance studies relative to the bulk sediment, which tends to average the magnetic properties of constituent fractions into a single value. Silt-size fractions are better suited for discrimination of Icelandic and southern Greenlandic sources as clay fractions frequently overlap in end-member space. Using silt M_{rs}/M_s and χ/χ_{273K} values sediment sources to core MD99-2227 on Eirik Ridge were successfully unmixed since the last glacial maximum. A major advantage of using χ/χ_{273K} curves was the ability to discriminate between the different crystallinity and cation substitution characteristics of the plutonic/metamorphic and volcanic sources that might otherwise have been difficult to isolate using other techniques. Required sample volumes are typically larger than those needed for VSM studies, however, the sensitivity of the χ/χ_{273K} dataset to subtle crystallographic variations makes it an attractive technique that is potentially applicable in a wide variety of environmental settings.

Acknowledgements

This research was supported by US National Science Foundation awards ANS-0902751 (Stoner), OCE-1636381 (Hatfield and Stoner), and NSF-EAR0421457 (Housen). This research was supported and

facilitated by an Institute of Rock Magnetism visiting fellowship to Hatfield. We would also like to thank Anders Carlson, Lisa Colville, Alberto Reyes, Sarah Strano, and Kelsey Winsor for assistance collecting sediment samples in Iceland and Greenland and Russ Burmester for help measuring the magnetic properties of the samples at Western Washington University. This manuscript was greatly improved by the reviews of Tilo von Dobeneck and Ramon Egli.

References

518	Bilardello, D., Jackson, M. 2013. What do the Mumpsies do? IRM Quarterly, 23-3
519	Chang, L., Roberts, A.P., Heslop, D., Hayashida, A., Li, J., Zhao, X., Tian, W., Huang, Q. 2016. Widespread
520	occurrence of silicate-hosted magnetic mineral inclusions in marine sediments and their
521	contribution to paleomagnetic recording, J. Geophys. Res. Solid Earth, 121, 8415–8431.
522	Channell, J.E.T. Harrison, R.J., Lascu, I., McCave, I.N., Hibbert, F.D., and Austin, W.E.N. 2016. Magnetic
523	record of deglaciation using FORC-PCA, sortable-silt grain size, and magnetic excursion at 26 ka,
524	from the Rockall Trough (NE Atlantic). Geochem. Geophys. Geosyst. 17, 1823-1841.
525	Channell, J.E.T., and Lehman, B. 1997. The last two gomagnetic polarity reversals recorded in high-
526	deposition-rate sediment drifts. Nature, 389, 712-175.
527	Carter-Stiglitz, B., Moskowitz, B., Solheid, P., Berquo, T.S., Jackson, M., and Kosterov, A. 2006. Low-
528	temperature magnetic behavior of multidomain titanomagnetites: TM0, TM16, and TM35 J.
529	Geophys. Res. Solid Earth, 111 (B12)
530	Day, R., Fuller, M., and Schmidt, V.A. 1977. Hysteresis properties of titanomagnetites: Grain size and
531	composition dependence, Physics of the Earth and Planetary Interiors, 13, pp. 260-267.
532	Dunlop, D.J. 2002. Theory and application of the Day plot (Mrs/Ms versus H _{cr} /H _c): 1. Theoretical curves
533	and tests using titanomagnetite data. J. Geophys. Res. 107, doi:10.1029/2001JB000486.
534	Egli, R., Chen, A.P., Winklhofer, M., Kodama, K.P., Horng, C-S. 2010. Detection of non-interacting single
535	domain particles using first-order. reversal curve diagrams. Geochem. Geophys. Geosyst. 11,
536	Q01Z11

537	Escher, J.C., Pulvertaft, T.C.R. 1995. Geological Map of Greenland 1:2,500,000. Geological Survey of
538	Greenland, Copenhagen.
539	Galindo-González, C., J.M. Feinberg, T. Kasama, L. Cervera Gontard, M. Pósfai, I. Kósa, J.D.G. Duran, J.E.
540	Gil, R.J. Harrison, and R.E. Dunin-Borkowski (2009). Magnetic and microscopic characterization of
541	magnetite nanoparticles adhered to clay surfaces, American Mineralogist 94, 1120-1129.
542	Gee, J., Kent, D.V. 1999. Calibration of magnetic granulometric trends in oceanic basalts. Earth Planet.
543	Sci. Lett. 170, 377–390.
544	Hatfield, R.G. 2014. Particle size-specific magnetic measurements as a tool for enhancing our
545	understanding of the bulk magnetic properties of sediments. Minerals, 4, 758-787.
546	Hatfield, R.G., Reyes, A.V., Stoner, J.S., Carlson, A.E., Beard, B.L., Winsor, K, and Welke, B. 2016.
547	Interglacial responses of the southern Greenland ice sheet over the last 430,000 years determined
548	using particle-size specific magnetic and isotopic tracers. Earth and Planetary Science Letters, 454,
549	225-236.
550	Hatfield, R.G., Stoner, J.S., Carlson, A.E., Reyes, A.V., and Housen B. 2013. Source as a controlling factor
551	on the quality and interpretation of sediment magnetic records from the northern North Atlantic.
552	Earth and Planetary Science Letters, 368, pp. 69-77.
553	Harrison, R. J., & Feinberg, J. M. (2008). FORCinel: An improved algorithm for calculating first-order
554	reversal curve distributions using locally weighted regression smoothing. Geochemistry,
555	Geophysics, Geosystems, 9(5), [Q05016].
556	Heslop, D. (2015) Numerical strategies for magnetic mineral unmixing. Earth-Science Reviews, 150, 256-
557	284.

558	Jackson, M., Moskowitz, B., Bowles, J. 2011. Interpretation pf Low-Temperature Data Part III: The
559	Magnetite Verwey Transition (Part A). IRM Quarterly, 20-4.
560	Jakobsson, S.P. 1972. Chemistry and distribution pattern of recent basaltic rocks in Iceland. Lithos 5,
561	365–386.
562	Kawamura, N., Ishikawa, N., and Torii, M. 2012. Diagenetic alteration of magnetic minerals in Labrador
563	Sea sediments (IODP Sites U1305, U1306, and U1307). Geochem. Geophys. Geosyst. 13, (8),
564	Q08013.
565	Kissel, C. 2005. Magnetic signature of rapid climatic variations in glacial North Atlantic, a review.
566	Comptes Rendus Geosciences 337(10-11), pp. 908–918.
567	Kissel, C., Laj, C., Labeyrie, L., Dokken, T., Voelker, A. and Blamart, D. 1999. Rapid climatic variations
568	during marine isotopic stage 3: magnetic analysis of sediments from Nordic Seas and North Atlantic
569	Earth and Planetary Science Letters 171(3), pp. 489–502.
570	Korstgard, J., Ryan, B., Wardle, R. 1987. The boundary between Proterozoic and Archaean crustal blocks
571	in Central West Greenland and Northern Labrador. Geological Society of London, Special
572	Publications 27, 247–259.
573	Lattard, D., Engelmann, R., Kontny, A., Sauerzapf, U. 2006. Curie temperatures of synthetic
574	titanomagnetites in the Fe-Ti-O system: Effects of composition, crystal chemistry, and
575	thermomagnetic methods. Journal of Geophysical Research, 111, B12S28.
576	Ludwig, P., R. Egli, S. Bishop, V. Chernenko, T. Frederichs, G. Rugel, S. Merchel, and M.J. Orgeira
577	(2013). Characterization of primary and secondary magnetite in marine sediment by combining
578	chemical and magnetic unmixing techniques, Global and Planetary Change 110, 321-339.

579	Miki, M., Taniguchi, A., Yokoyama, M., Gouzu, C., Hyodo, H., Uno, K., Zaman, H., Otofuji, Y-I. 2009.
580	Palaeomagnetism and geochronology of the Proterozoic dolerite dyke from southwest Greenland:
581	indication of low palaeointensity. Geophys. J. Int. 179, 18-34.
582	Moskowitz, B.M. 1993. High-Temperature Magnetostriction of Magnetite and Titanomagnetites. Journal
583	of Geophysical Research, 98, 359-371.
584	Moskowitz, B.M., Jackson, M. and Kissel, C. 1998. Low-temperature magnetic behavior of
585	titanomagnetites. Earth and Planetary Science Letters, 157, pp. 141–149
586	Moskowitz, B.M., Frankel, R.B., Bazylinski, D.A. 1993. Rock magnetic criteria for the detection of biogenic
587	magnetite. Earth and Planetary Science Letters, 120, 283-300.
588	Muxworthy, A.R., McClelland, E. 2000. Review of the low-temperature magnetic properties of magnetite
589	from a rock magnetic perspective. Geophys. J. Int. 140, 101-114.
590	Muxworthy, A.R., Heslop, D., Paterson, G.A., Michalk, D. 2011 A Preisach method for estimating absolute
591	paleofield intensity under the constraint of using only isothermal measurements: 2. Experimental
592	testing. Journal of Geophysical Research, 116, B04103.
593	Oches, E.A., Banerjee, S.K. 1996. Rock-magnetic proxies of climate change from loess-paleosol
594	sediments of the Czech Republic. Studia Geophysica et Geodaetica, 40, 287-300.
595	Özdemir, Ö., Dunlop, D.J. and Moskowitz, B.M. 1993. The effect of oxidation on the Verwey transition in
596	magnetite, Geophysical Research Letters, 20 (16), 1671-1674.
597	Özdemir, Ö., Dunlop, D., Moskowitz, B.M. 2002. Changes in remanence, coercivity, and domain state at
598	low temperature in magnetite. Earth and Planetary Science Letters, 194, 343-358.

599	Pedersen, A.K., Watt, M., Watt, W.S., Larsen, L.M. 1997. Structure and stratigraphy of the early tertiary
600	basalts of the Blosseville Kyst, East Greenland. J. Geol. Soc. London 154, 565–570.
601	Rasmussen, T.L., van Weering, T.C.E., Labeyrie, L., 1997. Climatic instability, ice sheets and ocean
602	dynamics at high northern latitudes during the last glacial period (58-10 KA BP). Quat. Sci. Rev. 16,
603	71–80
604	Reyes, A.V., Carlson, A.E., Beard, B., Hatfield, R.G., Stoner, J.S., Winsor, K., Welke, B., & Ullman, D.J.
605	(2014) South Greenland ice-sheet collapse during Marine Isotope Stage 11, Nature, 510, 525-528.
606	Roberts, A.P., Pike, C. and Verosub, K.L. 2000. First-order reversal curve diagrams: A new tool for
607	characterizing the magnetic properties of natural samples. Journal of Geophysical Research 105,
608	28,461-28,475.
609	Robinson, S.G. 1986. The late Pleistocene palaeoclimatic record of North Atlantic deep-sea sediments
610	revealed by mineral-magnetic measurements. Physics of The Earth and Planetary Interiors 42(1-2),
611	pp. 22–47.
612	Robinson, S.G., Sahota, J.T.S., Oldfield, F. 2000. Early diagenesis in North Atlantic abyssal plain sediments
613	characterized by rock-magnetic and geochemical indices. Marine Geology, 163, 77-107.
614	Smirnov, A. 2009. Grain size dependence of low-temperature remanent magnetization in natural and
615	synthetic magnetite: Experimental Study. Earth Planets Space, 61, 119-124.
616	Snowball, I., and Moros, M. 2003. Saw-tooth pattern of North Atlantic current speed during Dansgaard-
617	Oeschger cycles revealed by the magnetic grain size of Reykjanes Ridges sediments at 59°N.
618	Paleoceanography, 18 (2), 1026.
619	Stacey, F. D., and Banerjee, S. K. 1974. The Physical Principles of Rock Magnetism, volume 5 of
620	Developments in Solid Earth Geophysics. Elsevier Sci. Publ. Co.

621	Stoner, J.S., Channell, J.E.T. and Hillaire-Marcel, C. 1996. The magnetic signature of rapidly deposited
622	detrital layers from the Deep Labrador Sea: Relationship to North Atlantic Heinrich layers.
623	Paleoceanography 11(3), pp. 309.
624	Tauxe, L. 1998. Paleomagnetic Principles and Practice. Dordrecht: Kluwer Academic Publishers.
625	Thompson, R., Oldfield, F. 1986. Environmental Magnetism. Allen & Unwin, London.
626	Walz, F., Torres, L., Bendimya, K., de Francisco, C., Kronmuller, H. 1997. Analysis of magnetic after-effect
627	spectra in titanium-doped magnetite, Physica Status Solidi A, 164, 805–20.
628	Watkins, S.J. and Maher, B.A. 2003. Magnetic characterisation of present-day deep-sea sediments and
629	sources in the North Atlantic. Earth and Planetary Science Letters 214(3-4), pp. 379–394.
630	Willigers, B. J. A., van Gool, J.A.M., Wijbrans, R., Krogstad, J., Mezger, K.J. 2002. Post tectonic cooling of
631	the Nagssugtoqidian orogen and a comparison of contrasting cooling histories in Precambrian and
632	Phanerozoic orogens. J. Geol. 110, 503–517.
633	Worm, H-U. 1998. On the superparamagnetic-stable single domain transition for magnetite, and
634	frequency dependence of susceptibility. Geophys. J. Int. 133, 201-206.
635	Worm, H-U., and Jackson, M. 1999. The superparamagnetism of Yucca Mountain Tuff. Journal of
636	Geophysical Research, 104, 25415-25425.

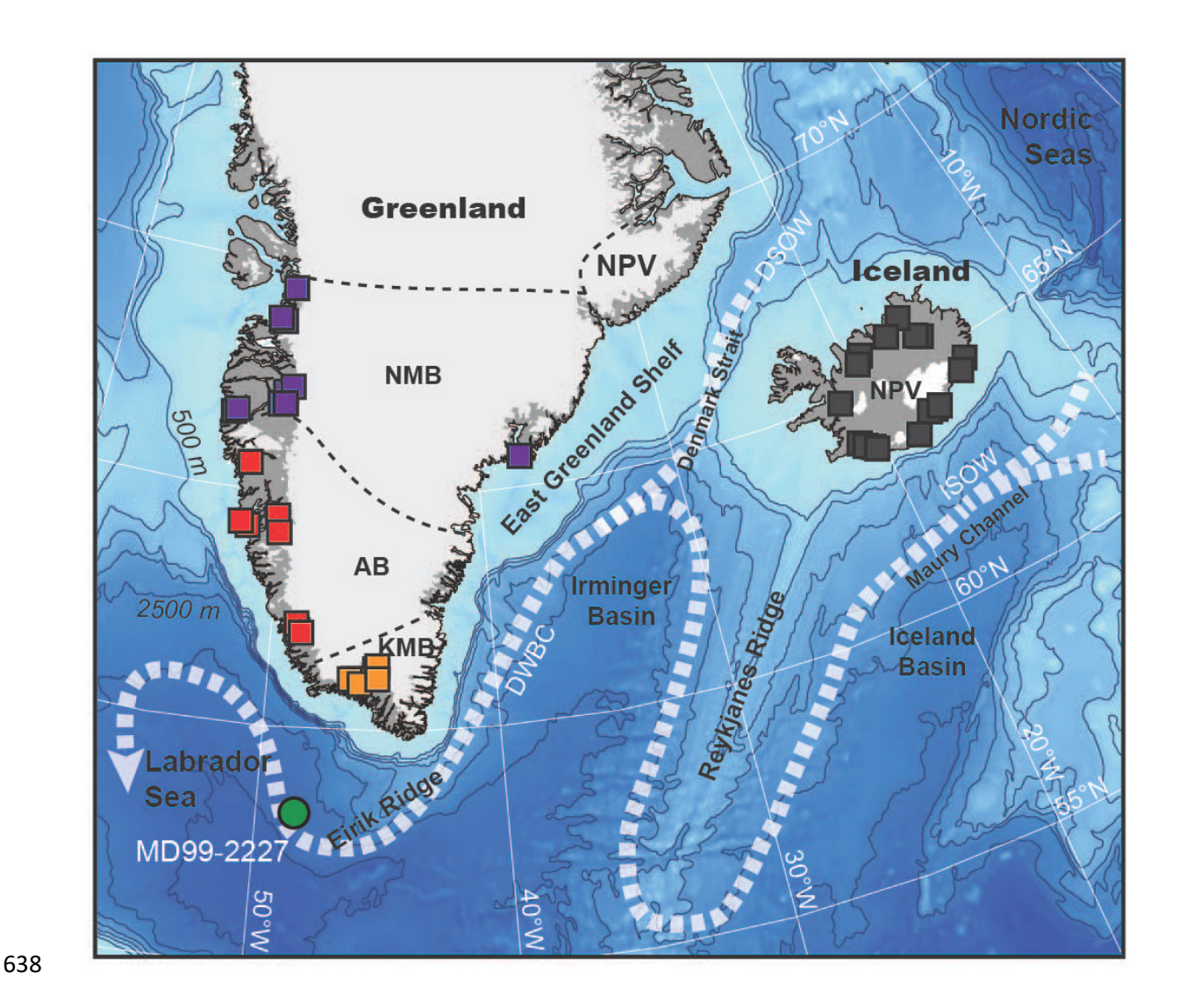


Figure 1: Location of terrestrial sediment samples from the Neogene and Paleocene volcanics (NPV) of Iceland (black squares), and the three terranes of southern Greenland; the Nagssustoqidian Mobile Belt (NMB; purple squares), Archean Block (AB; red squares), and Ketilidian Mobile Belt (KMB; orange squares). The location of core MD99-2227 (green circle) on the Eirik ridge is shown alongside the path of the Deep Western Boundary Current (DWBC) and its two major precursors, Denmark Strait Overflow Water (DSOW) and Iceland Scotland Overflow Water (ISOW). Bathymetry contours are at 500m intervals.

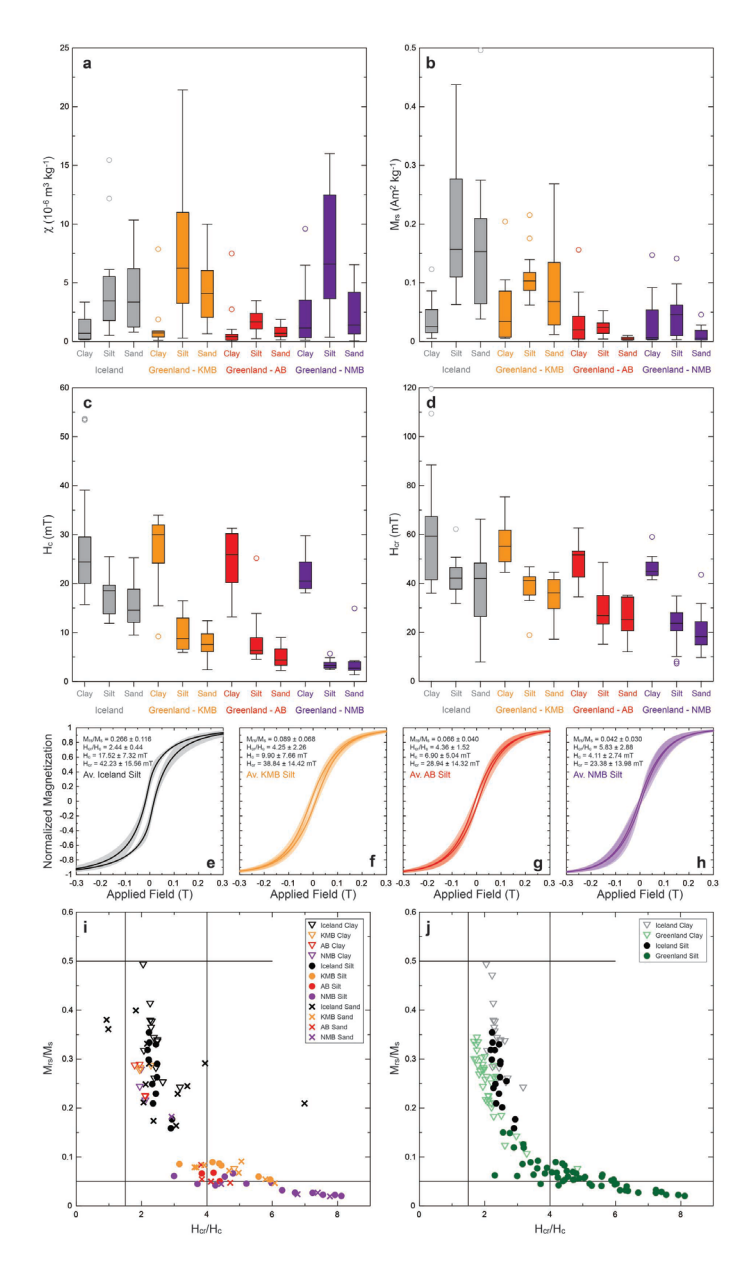


Figure 2: Box whisker plots of; (a) magnetic susceptibility (χ), (b) saturation remanent magnetization (M_{rs}), (c) coervicity (H_c), and (d) coervivity of remanence (H_{cr}). Each plot shows the median values (central line), interquartile range (boxed range), range of samples within 1.5x the interquartile range of the median (black bars), and outliers to this range (open circles) for clay, silt, and sand from Iceland and the three terranes of southern Greenland. Average silt-size fraction hysteresis loops (solid lines), after paramagnetic correction and normalization at 1000mT, are shown with their 2 standard deviation uncertainty (shading) and average (\pm 2 standard deviation range) parameters (text) for (e) Iceland (black), (f) KMB (orange), (g) AB (red), and (h) NMB (purple) terrestrial samples. Note the wider loops from Iceland contrast the thinner loops from southern Greenland that tighten from the KMB through the AB to the NMB. (i) Day plot (Day et al., 1977) of H_{cr}/H_c and M_{rs}/M_s ratios of Iceland, KMB, AB, and NMB clay (open triangles), silt (solid circles), and sand (crosses) fractions. (j) Integration of these data with those of Hatfield et al. (2013) to show the composite Greenland (green symbols) and Iceland terrestrial clay and silt dataset.

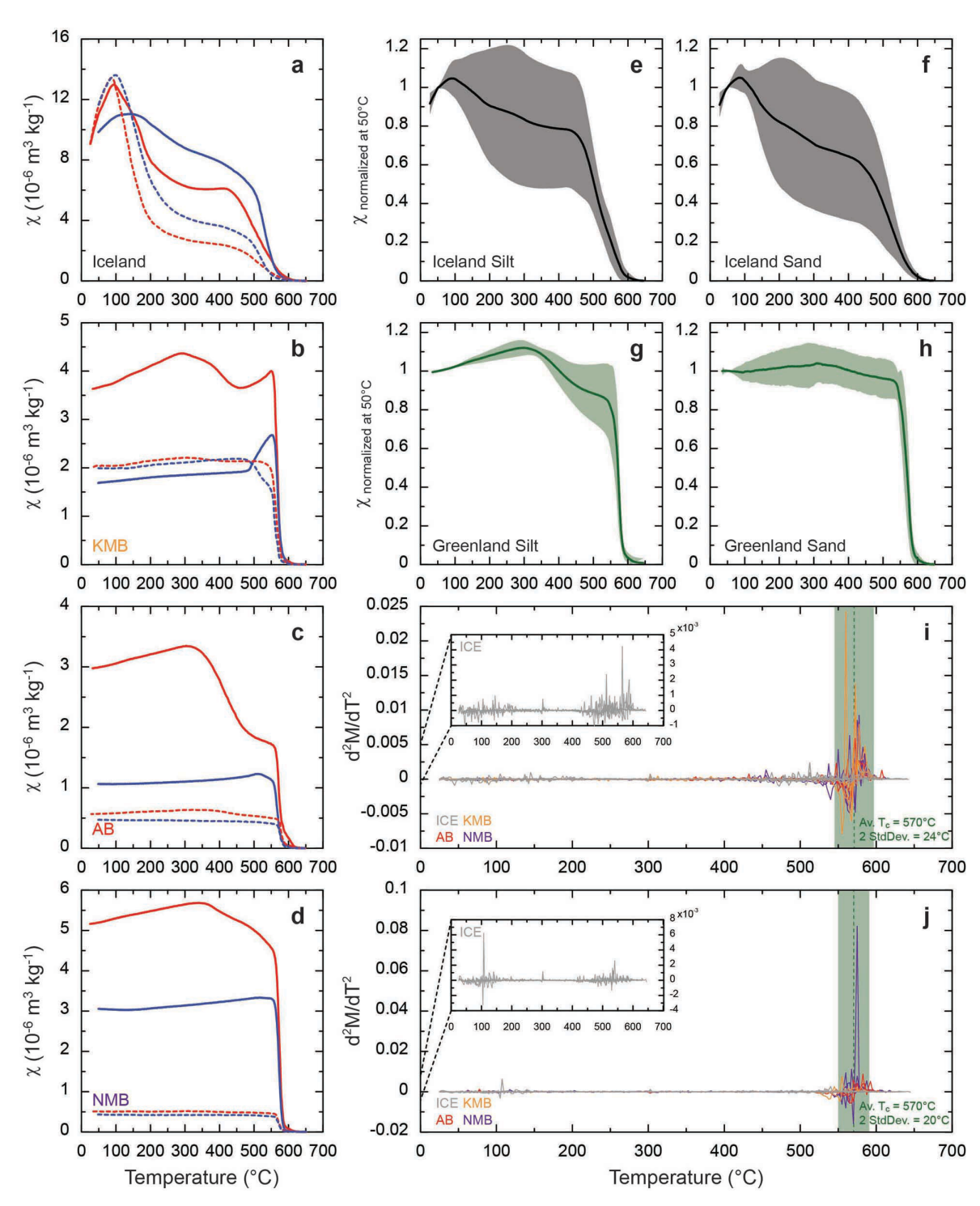


Figure 3: χ as a function of temperature between 25-650 °C for representative silt (solid lines) and sand (stippled lines) fractions from (a) Iceland, (b) the KMB, (c) AB, and (d) NMB. Red curves represent χ during heating, blue curves are χ values measured during cooling. Average (solid lines) and standard deviation (shading) of χ during heating normalized at 50°C for Iceland silt (e) and sand (f) and Greenland silt (g) and sand (h). Peaks in d^2M/dT^2 values of silt (i) and sand (j) samples from the KMB, AB, and NMB have relatively narrowly defined ranges (green bars) consistent with magnetite. Peaks in d^2M/dT^2 of Iceland samples (shown inset) occur at lower temperatures and are consistent with titanomagnetite.

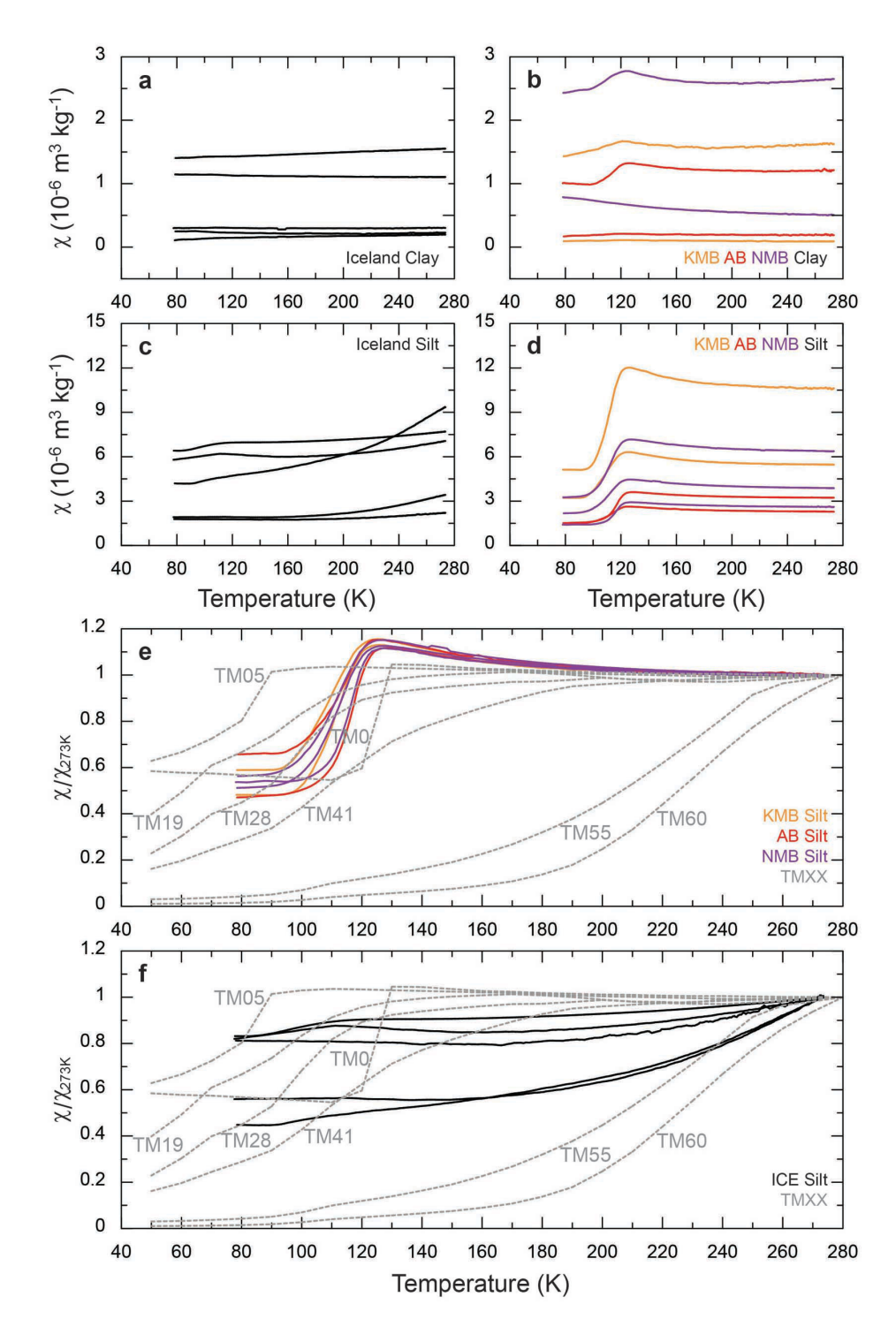


Figure 4: χ values as a function of temperature between ~80-273 K for clays (a-b) and silts (c-d) from Iceland (black) and the KMB (orange), AB, (red), and NMB (purple) from southern Greenland. Note the χ scale is five times higher for the silt samples than the clay samples. χ values normalized at 273 K (χ/χ_{273K}) for KMB, AB, and NMB silt (e) and Iceland silt (f) compared against χ/χ_{273K} of known compositions of (titano)magnetite TM0-TM60 (Moskowitz et al., 1998). While Greenland samples resemble the magnetite (TM0) curve Iceland samples are more similar to titanomagnetite curves over a range of different compositions.

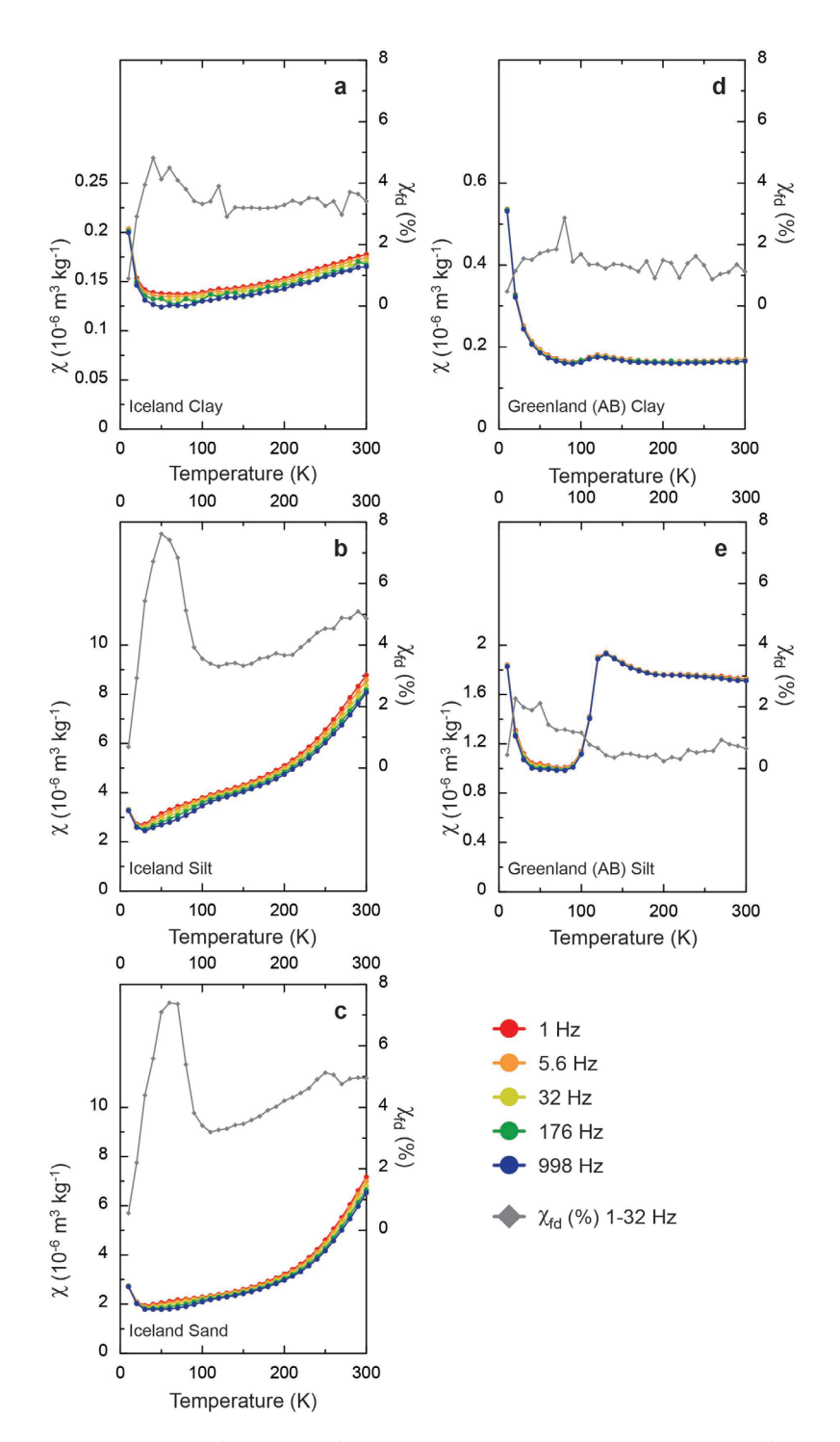


Figure 5: χ as a function of temperature between 10-300 K and frequency between 1-998 Hz (colored lines) for an Iceland clay (a), silt (b), and sand (c) and an AB clay (d) and silt (e) from Greenland. Frequency dependence of susceptibility (χ_{fd}) is shown for the difference between measurements at 1-32 Hz (gray crosses).

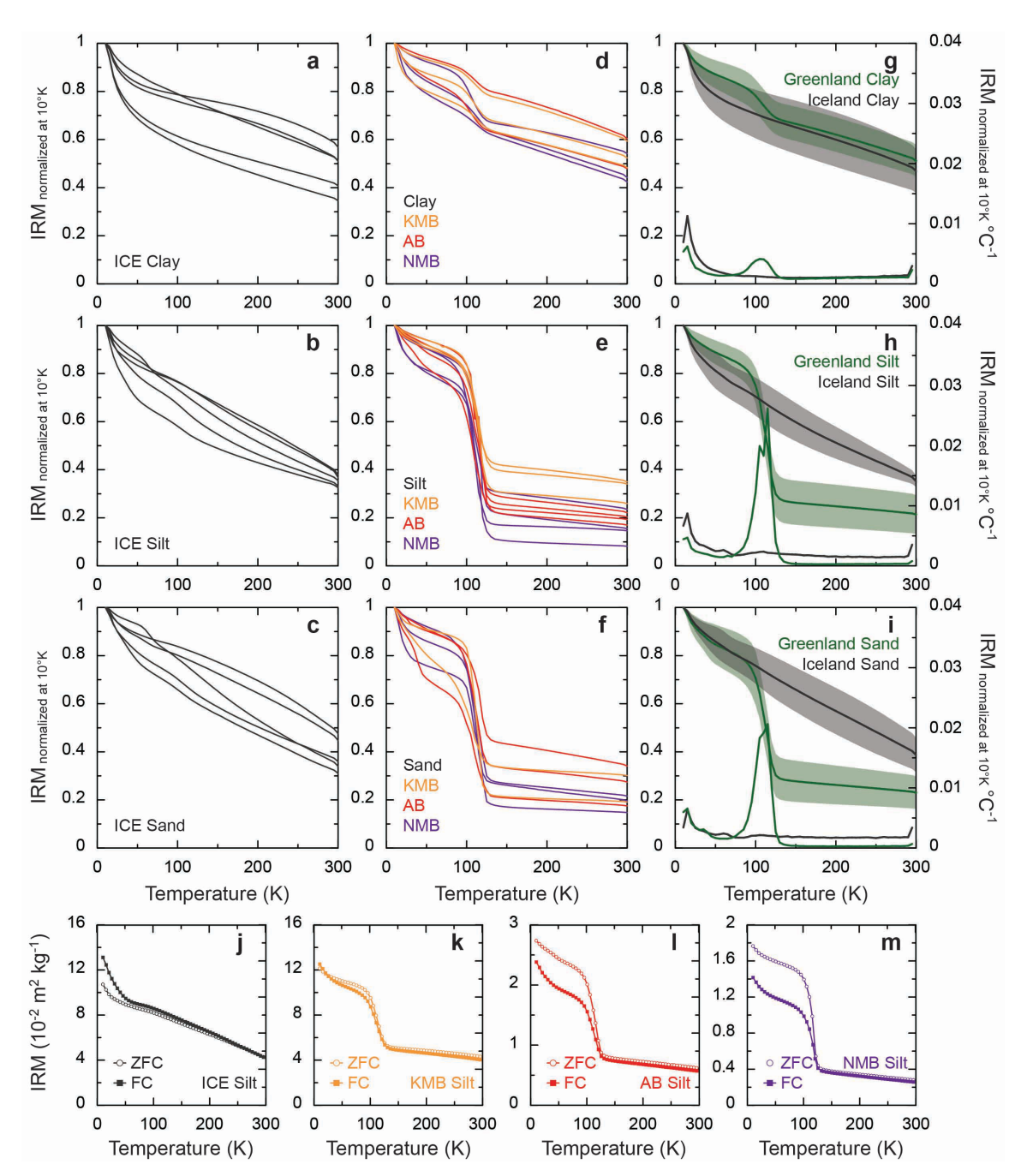


Figure 6: Zero field cooled (ZFC) remanence data between 10-300 K normalized to values at 10 K for Iceland clay (a), silt (b), and sand (c) and Greenland clay (d), silt (e), and sand (f). Average Greenland (green lines) and Iceland (black lines) profiles are shown with 1 standard deviation (shading) for clay (g), silt (h), and sand (i) fractions shown alongside the derivative showing rate of change of the normalized IRM per degree of temperature (stippled lines). Greenland samples show a Verwey (T_v) transition (sharp decrease in normalized IRM and peak in the derivative between 100-120 K), in contrast those from Iceland do not, instead showing more monotonic decreases in ZFC with increasing temperature. Comparisons of ZFC IRM (open circles) and field cooled (FC; solid squares) IRM for Iceland (j) and KMB (k), AB (l), and NMB (m) silt show greater ZFC than FC remanence below the T_v for the AB and NMB samples and near parity for the Iceland and KMB silts.

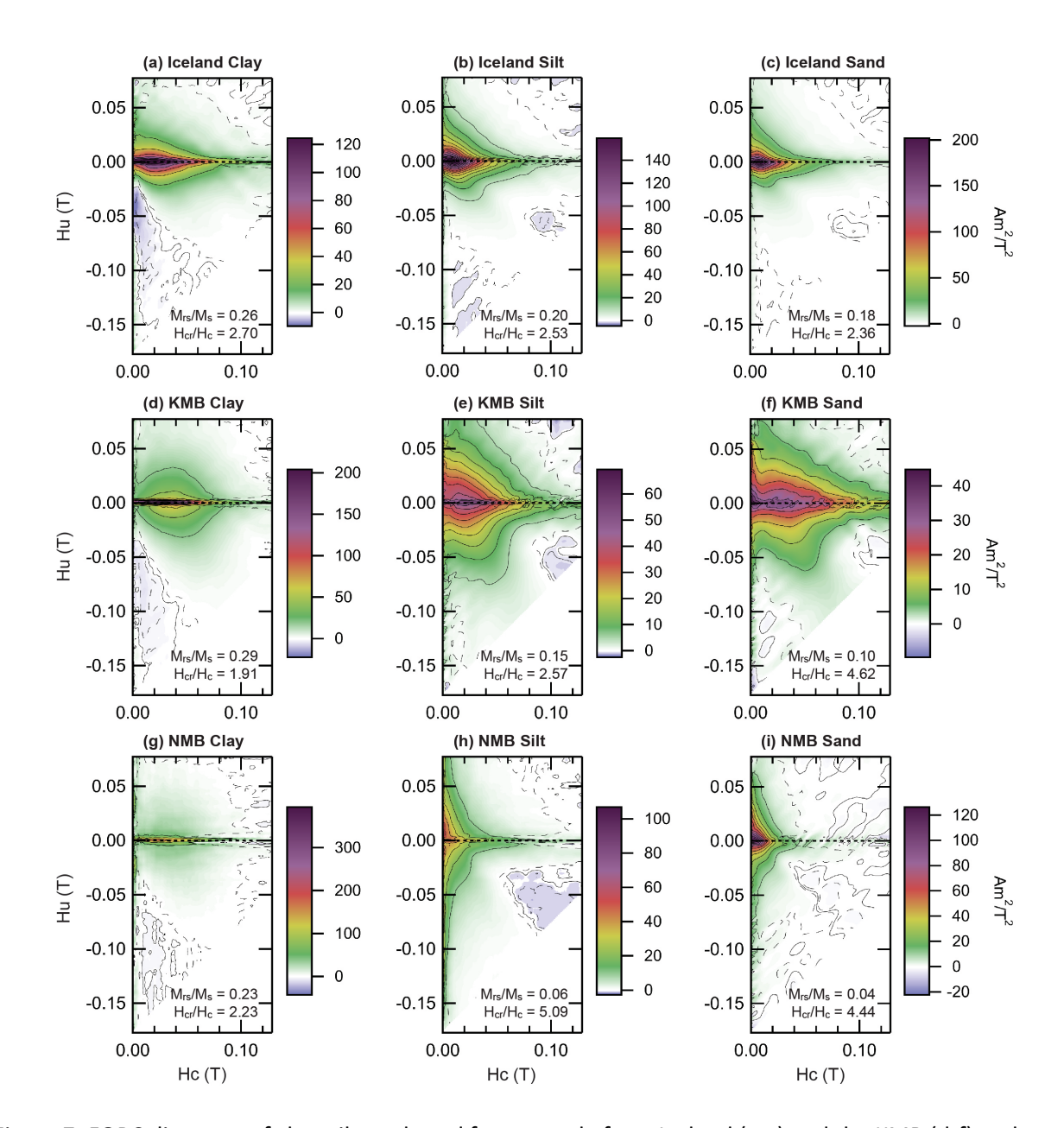


Figure 7: FORC diagrams of clay, silt, and sand for a sample from Iceland (a-c) and the KMB (d-f) and NMB (g-i) terranes from southern Greenland. Also shown are the corresponding M_{rs}/M_s and H_{cr}/H_c values determined from the major hysteresis loop shown in Figure 2i.

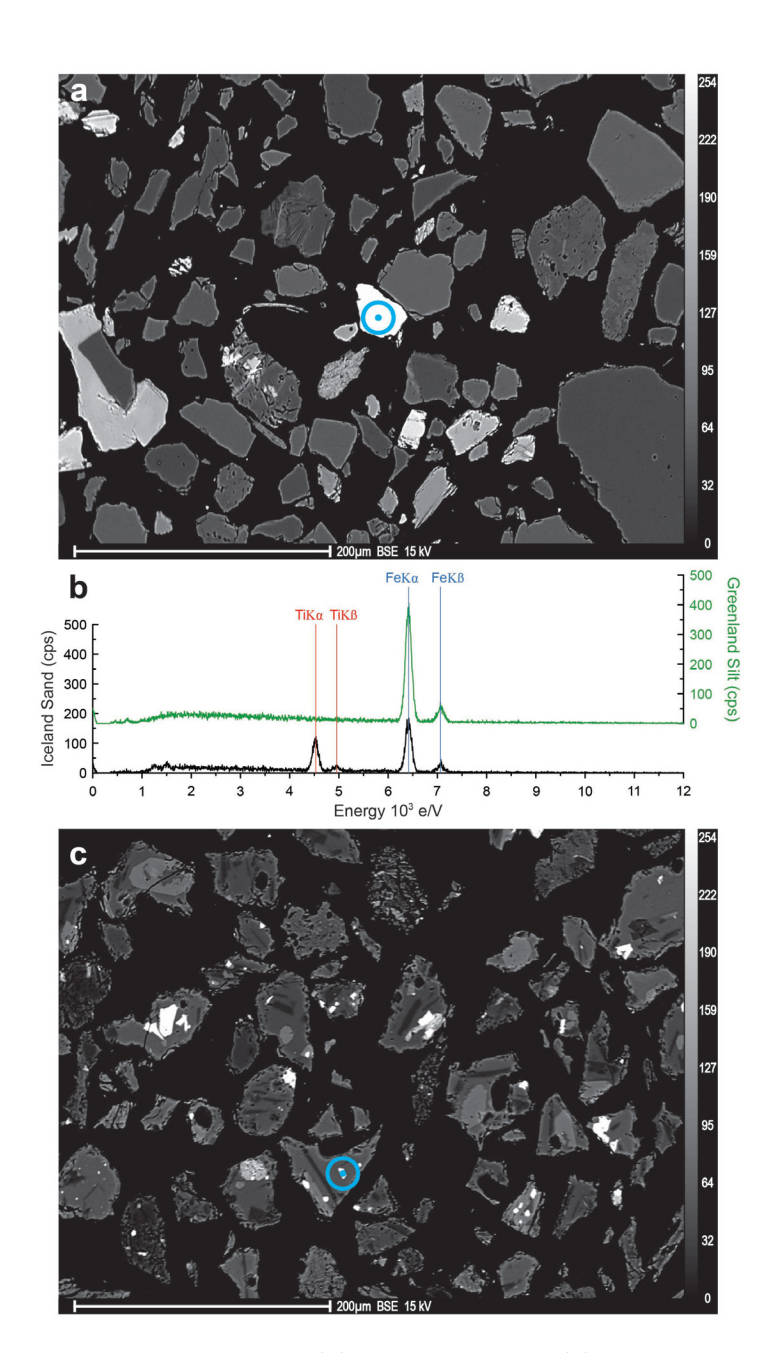


Figure 8: Greenland silt (a) and Iceland sand (c) electron backscatter images. White areas have higher mean atomic numbers and were evaluated using energy dispersive spectrometry (EDS) at the targeted sites (light blue targets) in (a) and (c) to produce the EDS spectra in (b). Note the discrete nature of iron (probably ferrimagnetic iron-oxides) in Greenland samples (green spectra) whereas smaller iron and titanium rich fragments from Iceland (black spectra) are held within a polycrystalline host matrix.

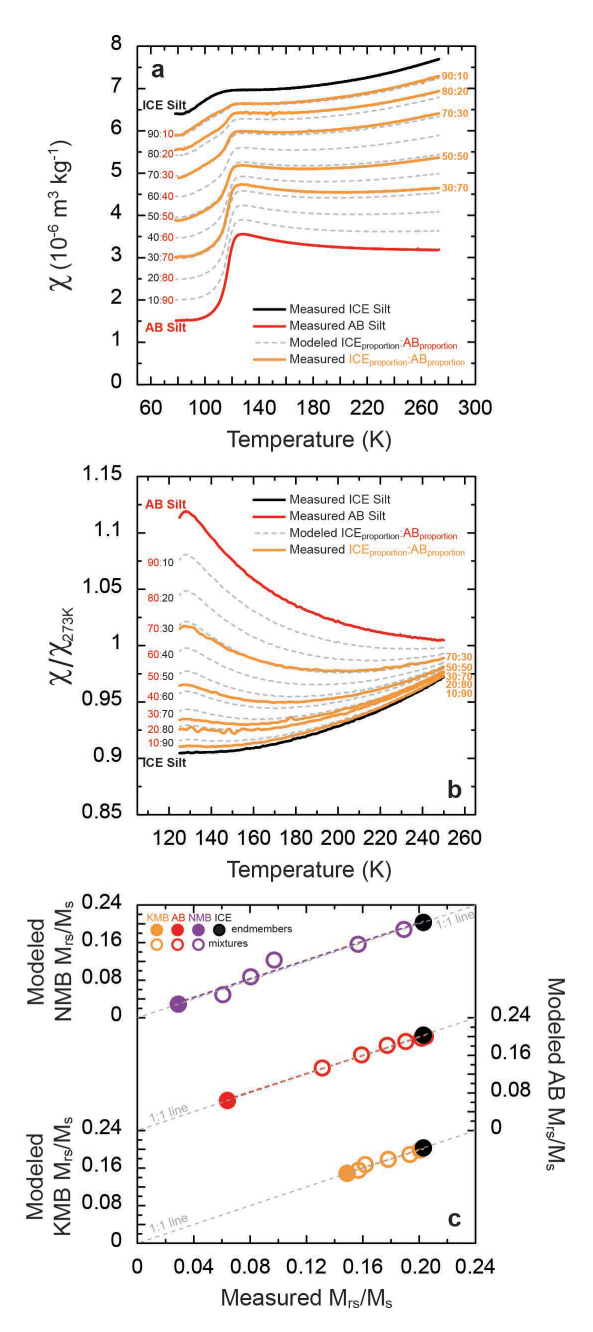


Figure 9: (a) χ values between ~80-273K for an AB silt (red) and an Iceland silt (black). Predicted values (grey dashed lines) result from linearly additive mixing between the two end-members using eq. 1. Measured mixtures of known proportions (orange lines) fall on top of the theoretical values for the same mixed proportion. (b) χ values normalized at 273K (χ/χ_{273K}) of the AB silt (red) and an Iceland silt (black) between 125-250 K. Predicted values (grey dashed lines) use the concentration corrected mixing of the two EMs (eq. 2) resulting in mixtures of known proportions (orange lines) plotting on top of the predicted values. (c) M_{rs}/M_s of a KMB silt (solid orange circle), an AB silt (solid red circle), and a NMB silt (solid purple circle) that were used as endmembers in mixtures with an Iceland silt (solid black circle). M_{rs}/M_s measurements of mixtures of known compositions (open circles using the same color scheme) match the modelled values predicted using eq. 2 and fall along respective 1:1 lines.

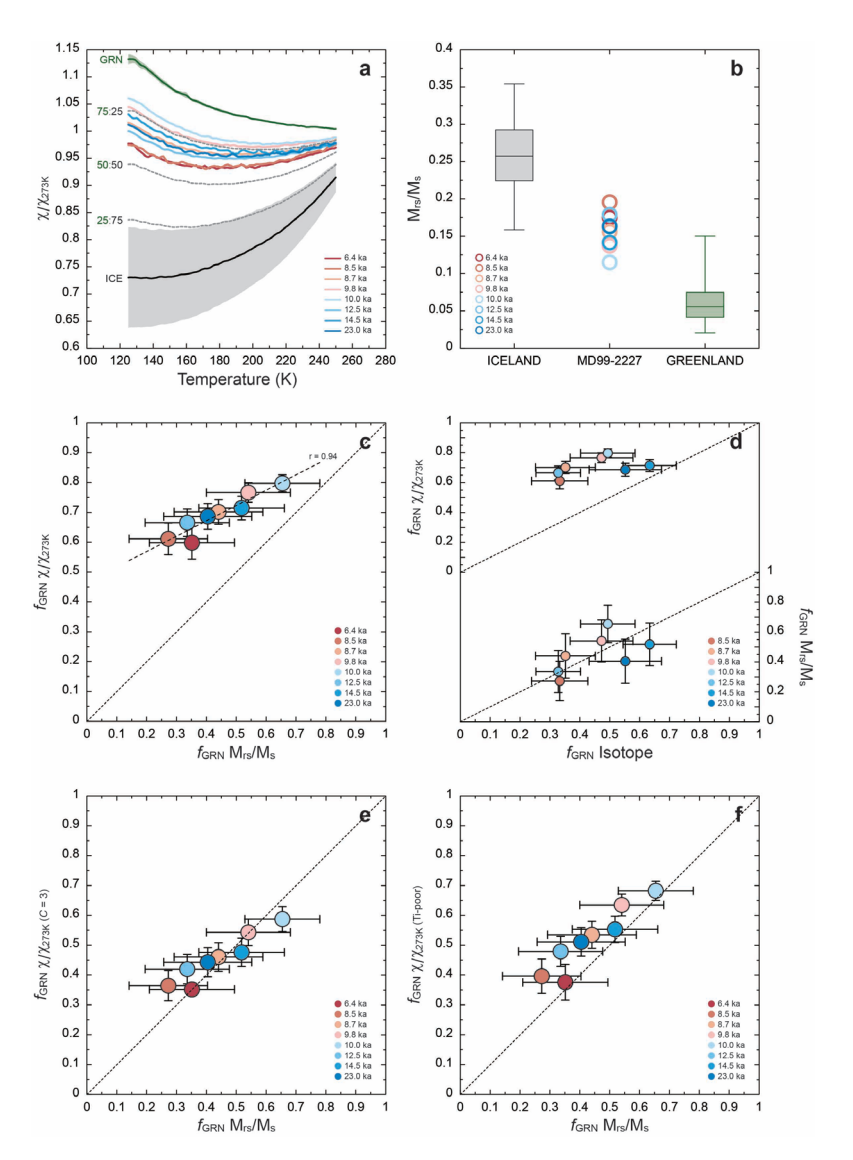


Figure 10: (a) Average χ/χ_{273K} end-member profiles for Greenland (solid green line) and Iceland (solid black line) silts between 125-250K realized using 10,000 randomly generated combinations of the measured χ/χ_{273K} profiles in Figure 4. Shading denotes the standard deviation around the average value and dashed grey lines show average estimated theoretical contributions after accounting for average end-member concentration differences. (b) Box whisker plots of 10,000 silt M_{rs}/M_s Iceland (black) and Greenland (green) end-members picked from a log-normal distribution of M_{rs}/M_s values; EM values generated outside of the observations in Fig. 2j were trimmed from the dataset. Measured χ/χ_{273K} profiles (colored lines in panel a) and M_{rs}/M_s values (open circles in panel b) of MD99-2227 silts fall between the respective EMs. (c) Greenlandic contributions (f_{GRN}) are unmixed separately for the χ/χ_{273K} data ($f_{GRN}\chi/\chi_{273K}$) and M_{rs}/M_s data ($f_{GRN}M_{rs}/M_s$) using eq. 3 and are shown with their standard deviation range. (d) Comparisons of $f_{GRN}M_{rs}/M_s$ and $f_{GRN}\chi/\chi_{273K}$ with independent f_{GRN} estimates from the isotope data (f_{GRN} Isotope) of Reyes et al. (2014) suggest that $f_{GRN}\chi/\chi_{273K}$ is overpredicted relative to $f_{GRN}M_{rs}/M_s$. Reconciliation of the two datasets in (c) can be achieved by fixing the C term in the f_{GRN} calculation of χ/χ_{273K} to a value of 3 (e), or by restricting the Iceland EM to include only Ti-poor profiles (f). The implications of each is discussed in the text.